enhan...d for a relativistic plasma (Beard, 1959). Imre (1962) has considered the problem of electromagnetic wave propagation in relativistic plasmas in detail. As an example, he obtains for propagation along the field, to first order in kT/mc^2,

$$\tilde{\mu}_{l,r}^2 \approx \frac{1-\dfrac{\omega_p^2}{\omega(\omega \pm \omega_b)}\left[1-\dfrac{5\omega}{2(\omega \pm \omega_b)}\dfrac{kT}{mc^2}\right]}{1+\dfrac{\omega\omega_p^2}{(\omega \pm \omega_b)^3}\dfrac{kT}{mc^2}}, \tag{3.6.1}$$

which is to be compared with (3.4.13). Johnston (1962) has developed weakly relativistic expansions, obtaining, for example, for electromagnetic waves in a plasma with no magnetic field

$$\tilde{\mu}^2 \approx \frac{1-\dfrac{\omega_p^2}{\omega^2}\left(1-\dfrac{5}{2}\dfrac{kT}{mc^2}\right)}{1+\dfrac{\omega_p^2}{\omega^2}\dfrac{kT}{mc^2}} \approx 1-\frac{\omega_p^2}{\omega^2}\left[1+\left(\frac{3}{2}-\frac{\omega_p^2}{\omega^2}\right)\frac{kT}{mc^2}\right], \tag{3.6.2}$$

which is to be compared with (3.4.22).

Exp #7

From Heald and Wharton
Plasma Diagnostics w/ Microwaves
Wiley 1965

CHAPTER 4

Wave propagation through bounded plasmas

4.1 Introduction

The preceding chapters have been concerned with the propagation of electromagnetic waves in an infinite plasma. We now consider the effect of plasma boundaries on the propagation. To study high-density discharges of arbitrary size and geometry, one is generally forced to use microwave beams directed through the plasma by means of suitable antenna systems. The alternative situation in which the plasma is located within a cavity or waveguide, or is itself a waveguide, is considered in Chapter 5. The "free-space" beam technique is favorable where the dimensions of the plasma are larger than the wavelength of an electromagnetic wave at the plasma frequency. Both classes of measurements are essentially limited to frequencies $\omega \gtrsim \omega_p$, the plasma frequency (except for special techniques exploiting a static magnetic field or a detailed independent knowledge of the density profile). Thus, the beam technique is most readily analyzed when

$$\omega^2 \gg \begin{cases} \omega_p^2, \\ (c/D)^2, \end{cases} \tag{4.1.1}$$

where D is the dimension of the plasma. The first of these two independent conditions permits convenient simplifications in the analysis by avoiding the plasma resonance; the second is essentially a diffraction condition which permits reducing the problem of propagation of a finite beam of electromagnetic waves through a finite plasma to a one-dimensional, plane-wave problem, as a first approximation.

The propagation constant of a microwave beam in a plasma has been shown, in Chapter 1, to depend upon the magnetic field, electron density, and collision frequency, and indirectly upon the temperature. The following basic arrangements, sketched schematically in Fig. 4.1, are useful in the case of high-temperature, highly ionized plasmas (that is, $\nu \ll \omega_p$).

(*1*) *Simple transmission or reflection.* For electron densities $n < n_c$ the plasma is transparent, while for $n > n_c$ it is opaque and totally reflecting, where $n_c = (\epsilon_0 m/e^2)\omega^2$ is the critical density.[1] The transition between

[1] In the presence of a magnetic field, the effective critical density may be altered. However, the situation is qualitatively unchanged.

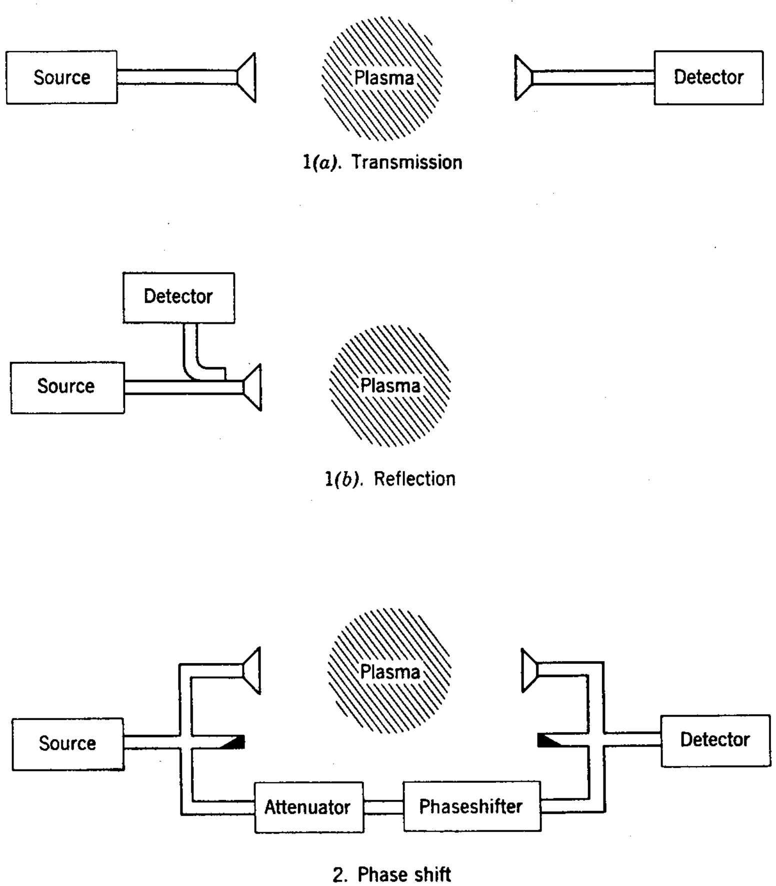

FIG. 4.1 Elementary microwave observation schemes.

these conditions is sharp. Thus, in principle, this elementary technique indicates whether the plasma density is above or below the critical value. Measurement at a given frequency is capable of determining only one value of density. The sharpness of the transition implied by the sudden change in the attenuation coefficient is not realized in practice because of the following factors.

(*a*) For densities below but approaching critical, the dielectric constant discontinuity at a sharp boundary produces an increasingly strong surface reflection (and corresponding reduction in transmission).

(*b*) If the plasma is only a few wavelengths thick, interference effects occur between the surface reflections.

(*c*) Inhomogeneous density distributions are not averaged in a simple manner.

(*d*) Refraction and scattering by the plasma occur because of inadequacies in the one-dimensional, plane-wave approximation.

If the plasma density is far above critical, an impinging signal is strongly reflected at the boundary. Therefore, motions of the effective boundary produce doppler shifts in the frequency of the reflected signal.

(*2*) *Phase shift* (*microwave bridge or interferometer*). If the signal from an auxiliary transmission path, with adjustable amplitude and phase elements, is balanced against the primary transmission signal to give a null in the absence of plasma, the output signal of the waveguide (hybrid) junction is a measure of the attenuation and phase shift in the primary path due to the plasma. In the fully transparent region of electron density, where $n \ll n_c$, a detected signal represents only phase shift which, in turn, is essentially a function of electron density only. Since the shift in phase can be calibrated, one has a continuous measurement of density between the upper limit of serious amplitude effects in the transmission path, and the lower limit of detector sensitivity. This technique is ideally suited to the observation of density as a function of time.

The propagation of the microwave beam through the bounded plasma is most readily analyzed in two limiting cases: first, the *gradual* boundary, with density varying slowly over a wavelength, to which an adiabatic analysis may be applied; and, second, the *sharp* boundary which can be attacked as a boundary-value problem. A formally similar situation occurs in quantum mechanics, in which the first case is known as the WKB approximation (Bohm, 1951). The usual *geometrical optics* limit partakes of both the above limits. It neglects reflections at the "sharp" boundaries which separate regions of different propagation characteristics and, thus, can be self-consistent only for plasmas large compared to a wavelength. The models of plasma geometry that are most useful for however, we do not restrict our consideration to this first-order case, but still retain the adiabatic approximation, we can (*1*) expand the $\Delta\phi$ integrand to higher orders, in which case the integrals obtained are higher-order averages of the distribution function (for example, $\int n^2(x)\,dx$); or (*2*) integrate $\Delta\phi$ directly using an appropriate distribution function.

In either case, a meaningful average electron density is not obtained without an independent knowledge of the distribution function, since the phase shift is not linear with density, and the method becomes less useful for the quantitative measurement of even average densities. If, for example, we assume a constant electron density (that is, a rectangular profile which, incidentally, is somewhat contradictory to the adiabatic assumption), the integration is trivial, and we obtain a parabolic dependence of density on phase shift

$$\frac{n}{n_c}=2\left(\frac{\lambda}{L}\frac{\Delta\phi}{2\pi}\right)-\left(\frac{\lambda}{L}\frac{\Delta\phi}{2\pi}\right)^2. \tag{4.2.10}$$

Figure 4.3 is a universal graph of this relation.

Since the phase shift introduced by the plasma sample is, in general, a nonlinear function of electron density, we obtain information on the distribution of density (profile) by making simultaneous measurements at different frequencies and/or with different polarizations with respect to a magnetic field.

We can expand the integrand in (4.2.2) (assuming no magnetic field),

$$\begin{aligned}\Delta\phi&=\int_0^L\left\{1-\left[1-\left(\frac{\omega_p}{\omega}\right)^2\right]^{1/2}\right\}\frac{2\pi}{\lambda}\,dx\\&=\int_0^L\left[\frac{1}{2}\frac{pn(x)}{\omega^2}+\frac{1}{8}\frac{p^2n^2(x)}{\omega^4}+\frac{1}{16}\frac{p^3n^3(x)}{\omega^6}+\frac{5}{128}\frac{p^4n^4(x)}{\omega^8}+\cdots\right]\frac{\omega}{c}\,dx,\end{aligned} \tag{4.2.11}$$

where $p=e^2/\epsilon_0 m$. Note that the series does not converge rapidly. As an example, consider two measurement frequencies

$$\omega_1=\omega$$
$$\omega_2=2\omega,$$

for which

$$\begin{aligned}\Delta\phi_1&=\frac{1}{2}\frac{p}{c\omega}\int n(x)\,dx+\frac{1}{8}\frac{p^2}{c\omega^3}\int n^2(x)\,dx+\frac{1}{16}\frac{p^3}{c\omega^5}\int n^3(x)\,dx+\cdots,\\ \Delta\phi_2&=\frac{1}{4}\frac{p}{c\omega}\int n(x)\,dx+\frac{1}{64}\frac{p^2}{c\omega^3}\int n^2(x)\,dx+\frac{1}{512}\frac{p}{c\omega^5}\int n^3(x)\,dx+\cdots.\end{aligned} \tag{4.2.12}$$

Therefore

$$\Delta\phi_1-2\,\Delta\phi_2=\frac{3}{32}\frac{p^2}{c\omega^3}\int n^2(x)\,dx+\frac{15}{256}\frac{p^3}{c\omega^5}\int n^3(x)\,dx+\cdots \tag{4.2.13}$$

and we obtain for the first two averages of the distribution

$$\frac{p}{c\omega}\int n\,dx=4\left\{\left[\Delta\phi_2-\frac{1}{6}(\Delta\phi_1-2\,\Delta\phi_2)\right]+\frac{1}{128}\frac{p^3}{c\omega^5}\int n^3\,dx+\cdots\right\} \tag{4.2.14}$$

$$\frac{p^2}{c\omega^3}\int n^2\,dx=\frac{32}{3}\left\{(\Delta\phi_1-2\,\Delta\phi_2)-\frac{15}{256}\frac{p^3}{c\omega^5}\int n^3\,dx-\cdots\right\}. \tag{4.2.15}$$

The usefulness of this approach is limited by the accuracy of the differential measurement $\Delta\phi_1-2\,\Delta\phi_2$. When this quantity can be successfully measured, (4.2.14) provides a refined evaluation of the average density and (4.2.15) an estimate of the mean-square density.

Procedures for obtaining profile information have been developed by Motley and Heald (1959) and by Wharton and Slager (1960). Wharton and Slager use only the magnetic-field-independent parallel-polarization case. Their data-reduction procedure is to calibrate the *peak* electron density by means of the cutoff of a "low-frequency" wave, and obtain information from the simultaneously observed phase shift of a "high-frequency" wave. Motley and Heald, using different polarizations, calibrate the *average* density with the high-frequency wave, infer profile from the low-frequency wave. Because of the greater phase-shift nonlinearity of the perpendicularly polarized wave near cyclotron resonance, the multiple polarization technique, when applicable, is somewhat more sensitive. The Wharton and Slager technique provides profile information only at the instants of time for which cutoff occurs; the Motley and Heald technique is limited to situations where the cyclotron frequency is comparable to the plasma frequency and is accurately known. Both methods benefit from additional phase-shift data channels at other frequencies and/or polarizations, at the expense of instrumentation and data-reduction complexity. Neither method is able to distinguish a hollow discharge from a peaked one. Experimental applications of these principles are discussed in Sections 6.4 and 6.5.

4.2.3 ***Reflections from cutoffs and resonances.*** Cutoffs, at which the index of refraction $\mu\to 0$, and resonances, at which $\mu\to\infty$, occur for certain combinations of frequency, density, and magnetic field. When a wave propagating in an inhomogeneous plasma impinges upon regions having these special characteristics, reflection and absorption must be considered even in the adiabatic approximation. Near the cutoff, the wavelength grows large, while near the resonance the wavelength becomes small. In both cases, the group velocity goes to zero. The analysis of this situation is formally identical to that resulting in the so-called turning-point connection formulas of the quantum-mechanical WKB approximation (Schiff, 1955). It can be shown that in the case of a *cutoff* the wave is *reflected* from the anomalous region with little dissipation (Denisov, 1958; Stix, 1960). The external behavior is thus very similar to that of a sharply bounded, high-density ($n > n_c$) plasma. In the case of a *resonance*, however, the wave is largely *absorbed*. This distinction is of considerable significance for both reflection-type microwave probing measurements

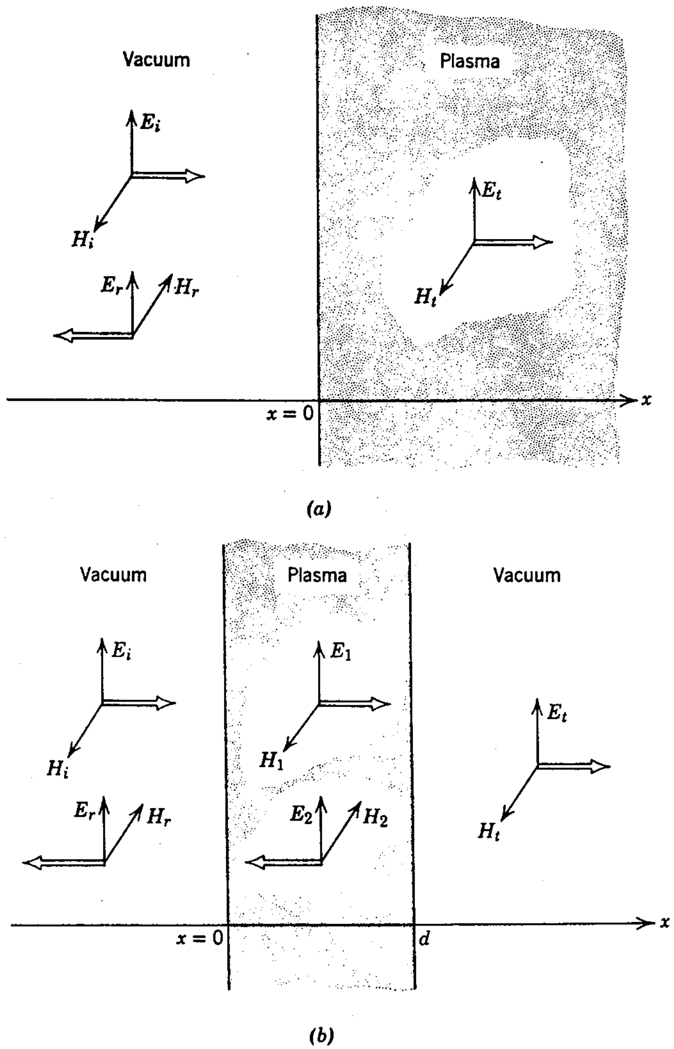

FIG. 4.4 Reflection and transmission at sharp boundaries. (*a*) Vacuum-plasma interface. (*b*) Plasma slab.

and thermal radiation measurements, as well as for the nondiagnostic question of plasma heating by electromagnetic radiation.

It will be noted from the graphs of Chapter 1 that, in general, for a given magnetic field, cutoff occurs at a lower density than the resonance. Thus, characteristically, waves entering the plasma from outside are reflected before reaching the resonance. The resonance may, in some cases, be made accessible by allowing the wave to enter the plasma in a region of high magnetic field (generally such that the cyclotron frequency $\omega_b > \omega$) which then decreases spatially within the plasma, so that the resonance is approached from the high-field side. In Section 6.5.4 an experiment using this technique is described. A situation of this sort has been exploited in the "magnetic beach" geometry for the dissipation of ion-cyclotron waves (Stix, 1958). If the regions of cutoff and resonance are close together within the plasma, relative to a wavelength, it may be possible for a sort of "tunnel effect" to occur in which the resonance region extracts energy from the evanescent wave passing through the cutoff. Tunneling or "bridging" may also take place by mode conversion processes (Ratcliffe, 1959, Chapter 17). Stix (1960, 1962) has shown that at a resonance high-temperature and ion-mass effects may reduce absorption, increase reflection, and excite other plasma modes.

4.3 The slab with sharp boundaries

We again consider the interaction of a plane wave with a slab plasma. However, in contrast with the adiabatic case of Section 4.2, we now assume a homogeneous plasma with sharp boundaries, that is, the transition between vacuum and uniform plasma occurs over a distance much less than a wavelength. There exists a well-defined reflection coefficient at each interface, and reflection and transmission coefficients are determined by boundary conditions on the wave fields at the interfaces.

Consider first the single interface of Fig. 4.4*a*. Waves traveling to the right are represented by the phase factor $\exp(j\omega t - \breve{\gamma}x)$, and waves to the left, by $\exp(j\omega t + \breve{\gamma}x)$ where $\breve{\gamma} = \alpha + j\beta = (j\omega/c)\breve{\kappa}^{1/2}$ is the complex propagation constant. In the case of a plasma, the complex dielectric constant $\breve{\kappa}$, and hence $\breve{\gamma}$, are known functions of electron density, collision frequency, magnetic field, etc., as developed in Chapter 1. In accordance with Maxwell's equations, the magnitudes of the electric and magnetic wave fields are related by the wave impedance

$$\breve{\eta} = \frac{E}{H} = \left(\frac{\mu_0}{\breve{\kappa}\epsilon_0}\right)^{1/2}, \tag{4.3.1}$$

with respective polarizations as shown in the figure. The wave impedance $\breve{\eta}$ is, in general, complex on account of $\breve{\kappa}$. Since the waves are transverse and there are no surface currents at the interface, the boundary conditions require that E and H are continuous across the interface. Therefore the wave amplitudes, in the notation of Fig. 4.4*a*, are related by

$$E_i + E_r = E_t$$
$$E_i - E_r = \breve{\kappa}^{1/2} E_t. \qquad (4.3.2)$$

It follows that the (complex) *amplitude* reflection and transmission coefficients are, respectively,

$$\breve{\rho} = \frac{E_r}{E_i} = \frac{1-\breve{\kappa}^{1/2}}{1+\breve{\kappa}^{1/2}} = \frac{\breve{\eta}-\eta_0}{\breve{\eta}+\eta_0},$$
$$\breve{\tau} = \frac{E_t}{E_i} = \frac{2}{1+\breve{\kappa}^{1/2}} = \frac{2\breve{\eta}}{\breve{\eta}+\eta_0} \qquad (4.3.3)$$

where $\eta_0 = 377$ ohms is the wave impedance of free space. Note the significance of the wave impedance that there is no reflection when the impedances of the two media are equal.[2]

The single-interface *power* reflection and transmission coefficients are, respectively,

$$r = |\breve{\rho}|^2 = \frac{(1-\mu)^2+\chi^2}{(1+\mu)^2+\chi^2},$$
$$t = 1 - r = \mu|\breve{\tau}|^2 = \frac{4\mu}{(1+\mu)^2+\chi^2} \qquad (4.3.4)$$

where $\mu - j\chi = \breve{\kappa}^{1/2} = -j\breve{\gamma}c/\omega$, and the voltage standing-wave ratio is[3]

$$\mathrm{VSWR} = \frac{1+|\breve{\rho}|}{1-|\breve{\rho}|} = \frac{1+r^{1/2}}{1-r^{1/2}}. \qquad (4.3.5)$$

[2] In a more general (nonplasma) case with the relative permeability κ_m different from unity and perhaps also complex, then $\eta = (\kappa_m \mu_0/\kappa\epsilon_0)^{1/2}$. Reflection at the interface between two media is suppressed so long as the ratio κ_m/κ is the same for both media, even though κ and κ_m themselves change by large factors. This effect is exploited in the design of microwave-absorbing wall coatings in which both κ and κ_m have imaginary (lossy) components (see Chapter 10).

[3] When the imaginary component of κ is negligible, the $\mathrm{VSWR} = 1/\kappa^{1/2} = 1/\mu = \eta/\eta_0$. The positive sense of polarization of the reflected wave has been chosen arbitrarily for the case $\kappa < 1$. If $\kappa > 1$, the sense of E_r is reversed and $\mathrm{VSWR} = \kappa^{1/2} = \mu = \eta_0/\eta$. We note, in passing, a convenient procedure for calculating the maximum transmission loss due to reflection. From standard transmission-line theory the maximum VSWR from two discontinuities is the product of the respective VSWR's (and the minimum, the quotient). Thus, the maximum transmission loss due to reflection from a slab can be obtained from standard charts assuming a single discontinuity with

$$\mathrm{VSWR} = \begin{cases} 1/\mu^2 & \mu < 1 \\ \mu^2 & \mu > 1. \end{cases}$$

This procedure applies only if there is no dissipative loss between discontinuities.

The situation of practical interest is that of the slab of Fig. 4.4*b*. By setting up boundary conditions similar to (4.3.2) at the two interfaces (or, alternatively, summing the infinite series of internally reflected waves), one finds (Stratton, 1941) the *amplitude* reflection and transmission coefficients

$$\breve{\Gamma} = \frac{E_r}{E_i} = \frac{\breve{\rho}[1-\exp(-2\breve{\gamma}d)]}{1-\breve{\rho}^2\exp(-2\breve{\gamma}d)}, \qquad (4.3.6)$$

$$\breve{T} = \frac{E_t}{E_i} = \frac{(1-\breve{\rho}^2)\exp[-(\breve{\gamma}-j\omega/c)d]}{1-\breve{\rho}^2\exp(-2\breve{\gamma}d)}, \qquad (4.3.7)$$

and the *power* reflection, transmission, and absorption coefficients are

$$R = \frac{r\{[1-\exp(-2\alpha d)]^2 + 4\exp(-2\alpha d)\sin^2(\beta d)\}}{[1-r\exp(-2\alpha d)]^2 + 4r\exp(-2\alpha d)\sin^2(\beta d - \psi)}, \qquad (4.3.8)$$

$$T = \frac{[(1-r)^2 + 4r\sin^2\psi]\exp(-2\alpha d)}{[1-r\exp(-2\alpha d)]^2 + 4r\exp(-2\alpha d)\sin^2(\beta d - \psi)}, \qquad (4.3.9)$$

$$A = 1 - R - T, \qquad (4.3.10)$$

where ψ is the phase angle of $\breve{\rho} = |\breve{\rho}|\exp(j\psi)$ and

$$r^{1/2}\sin\psi = \frac{2\chi}{(1+\mu)^2+\chi^2},$$
$$r^{1/2}\cos\psi = \frac{1-\mu^2-\chi^2}{(1+\mu)^2+\chi^2}. \qquad (4.3.11)$$

It is to be noted that the coefficients (4.3.8) to (4.3.10) are oscillatory functions of slab thickness d (or of frequency ω) as a result of interference of internally reflected waves. Likewise, the phase of the transmitted wave, which may be calculated from (4.3.7), is perturbed by interference. As a simplification, we may assume that the reflected waves are incoherent, thereby suppressing interference effects, and obtain[4]

[4] Interference is suppressed by considering only power relations. The fraction r of the incident wave is reflected at the first surface of the slab, the fraction $a(1-r)$ [where $a = \exp(-2\alpha d)$ is the one-way power loss through the slab] is transmitted to the second surface. Of this latter the fraction $a(1-r)^2$ escapes while the fraction $ar(1-r)$ is reflected back toward the first surface. Iteration of this analysis yields the series

$$R = r + a^2 r(1-r)^2(1 + a^2r^2 + a^4r^4 + \dots)$$
$$T = a(1-r)^2(1 + a^2r^2 + a^4r^4 + \dots).$$

Summation of these infinite series leads to (4.3.12) and (4.3.13).

$$R=\frac{r[1+(1-2r)\exp(-4\alpha d)]}{1-r^2\exp(-4\alpha d)}, \tag{4.3.12}$$

$$T=\frac{(1-r)^2\exp(-2\alpha d)}{1-r^2\exp(-4\alpha d)}, \tag{4.3.13}$$

$$A=\frac{(1-r)[1-\exp(-2\alpha d)]}{1-r\exp(-2\alpha d)}. \tag{4.3.14}$$

These latter relations are often useful for estimating average effects and become more realistic as $d \gg \lambda$. One may also be concerned with the case of oblique incidence, in which case the wave polarization becomes important (Graf and Bachynski, 1961).

Numerical calculations of (4.3.8) to (4.3.10) may readily be made as a function of plasma properties (French, Cloutier, and Bachynski, 1961). Figure 4.5 illustrates the case for a plasma four wavelengths thick. Figure 4.6 shows, for the same case, the phase error of the transmitted wave relative to the geometrical optics phase.

This sharp-boundary, homogeneous-plasma analysis can be extended to cylindrical geometry by expanding the incident and diffracted waves in terms of the normal-mode waves of the dielectric cylinder (Dawson and Oberman, 1959; Platzman and Ozaki, 1960). For electric-vector polarization perpendicular to a small plasma column, scattering resonances related to the plasma properties and geometry are found (Crawford et al., 1963). The finite size also modifies the frequency of longitudinal plasma oscillations (Branch and Mihan, 1955). Unless simplifying approximations can be made, numerical calculations for given experimental situations are usually difficult to carry out, even with electronic computers, since extensive summations over Bessel functions must be performed for each point. Calculation is especially difficult when the plasma diameter is not much larger than the wavelength, and when the receiving antenna is at a finite distance and subtends a nonzero angle at the plasma axis. The interaction of nearby antennas with sharp plasma boundaries, with resulting modification of reflection and transmission characteristics, has been studied in connection with precision interferometry (Kerns and Dayhoff, 1961) and with antenna matching (Redheffer, 1949).

4.4 Inhomogeneous plasmas

If the propagation properties of a plasma vary sufficiently slowly over a wavelength, the adiabatic analysis of Section 4.2 is applicable. However, this analysis explicitly excludes reflections and interference effects. At the other extreme, the case of a sharply bounded, homogeneous plasma may be solved by boundary-value methods, as outlined in Section 4.3. The treatment of the intermediate case between these two limits, especially

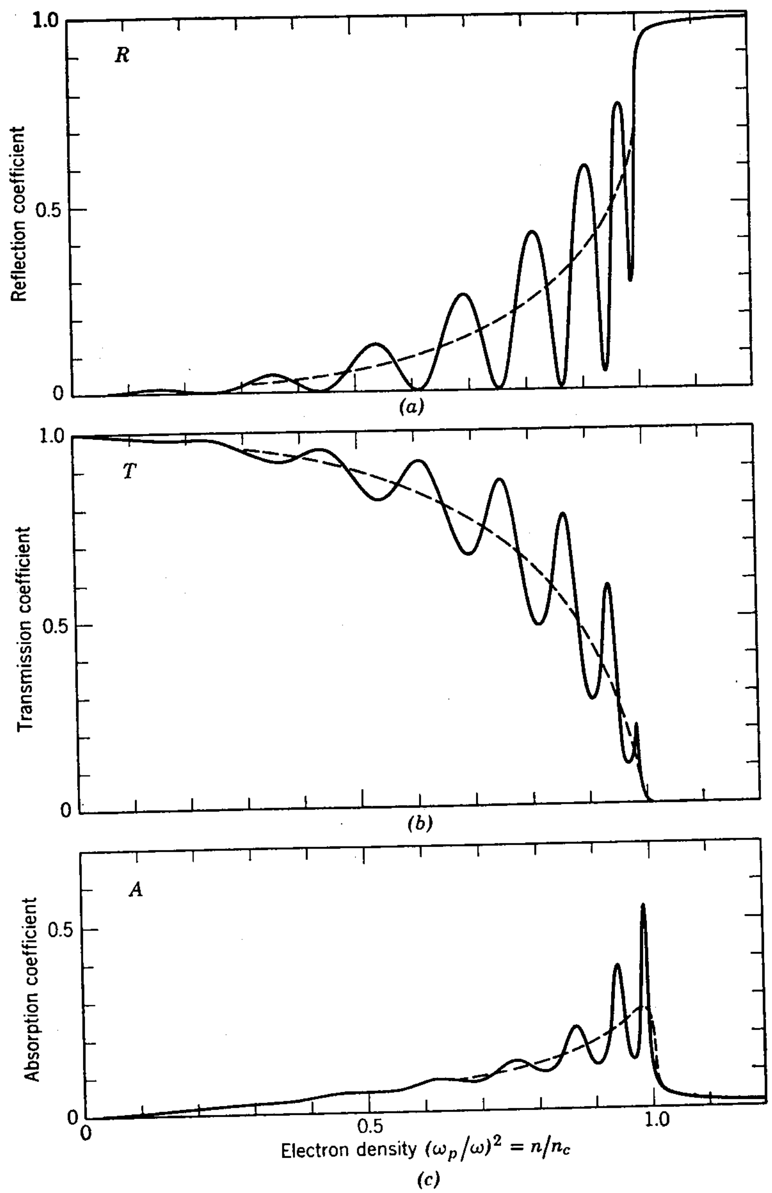

FIG. 4.5 Power reflection, transmission, and absorption coefficients, from (4.3.8) to (4.3.10), for a homogeneous slab plasma four wavelengths thick ($\nu/\omega = 0.003$). The dashed curves assume incoherent internal reflections, from (4.3.12) to (4.3.14).

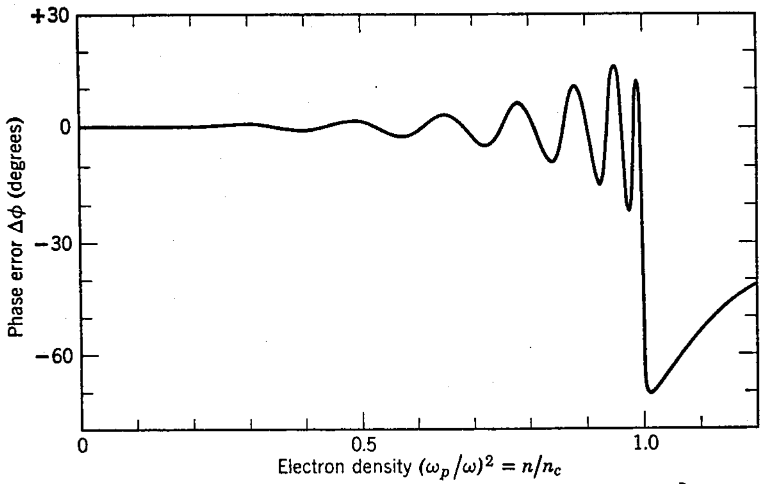

FIG. 4.6 Phase error of the transmitted wave, relative to the geometrical optics phase, for the same case as Fig. 4.5.

in the presence of a static magnetic field, is much more complicated since propagation in an inhomogeneous medium must be considered explicitly in terms of Maxwell's equations. In general, a-c spacecharge exists in regions of electron density gradients (Buchsbaum and Brown, 1957). For cold plasmas and for wavelengths long compared to interparticle distances and gyration radii, the local electromagnetic properties of the plasma medium may usually be represented by a space-dependent, complex dielectric constant $\breve{\boldsymbol{\kappa}}(\mathbf{r})$, which is a tensor quantity on account of the anisotropy introduced by a static magnetic field (Drummond, Gerwin, and Springer, 1961). Hence, for fields varying as $\exp j\omega t$, Maxwell's equations become

$$\nabla\times\mathbf{E} = -j\omega\mu_0\mathbf{H} \tag{4.4.1}$$

$$\nabla\times\mathbf{H} = j\omega\epsilon_0\breve{\boldsymbol{\kappa}}\cdot\mathbf{E} \tag{4.4.2}$$

$$\nabla\cdot(\breve{\boldsymbol{\kappa}}\cdot\mathbf{E}) = 0 \tag{4.4.3}$$

$$\nabla\cdot\mathbf{H} = 0. \tag{4.4.4}$$

Taking the curl of (4.4.1) and using (4.4.2), we obtain the wave equation for **E** in the form

$$\nabla\times\nabla\times\mathbf{E} = \frac{\omega^2}{c^2}\breve{\boldsymbol{\kappa}}\cdot\mathbf{E}. \tag{4.4.5}$$

The vector identity $\nabla\times\nabla\times\mathbf{E} = \nabla(\nabla\cdot\mathbf{E}) - \nabla^2\mathbf{E}$ allows us to rewrite the equation for **E** as

$$\nabla^2\mathbf{E} + \frac{\omega^2}{c^2}\breve{\boldsymbol{\kappa}}\cdot\mathbf{E} = \nabla(\nabla\cdot\mathbf{E}), \tag{4.4.6}$$

where in general the term on the right-hand side cross-couples the three components of **E**. Similarly, multiplying (4.4.2) by $\breve{\boldsymbol{\kappa}}^{-1}$, then taking its curl and using (4.4.1), we obtain the corresponding wave equation for **H** in the form

$$\nabla\times[\breve{\boldsymbol{\kappa}}^{-1}\cdot(\nabla\times\mathbf{H})] - \frac{\omega^2}{c^2}\mathbf{H} = 0. \tag{4.4.7}$$

Thus, either anisotropy or inhomogeneity causes the wave equations for **E** and **H** to be different and to contain terms which cross-couple the scalar field components. In the nonhomogeneous case, the difference arises physically from the fact that the wave impedance (that is, the ratio of E to H) changes even when the Poynting vector (the product of E and H) is approximately constant.

From (4.4.6) and (4.4.7) one can deduce the nature of initially plane waves for various assumed forms of dielectric constant, directions of inhomogeneity, and directions and polarizations of the waves (Bachynski, 1960). The results are summarized in Table 4.1. For instance, even in the absence of a magnetic field, a wave propagating perpendicular to the density gradient is no longer transverse electromagnetic (TEM).

4.4.1 ***Isotropic inhomogeneous plasmas.*** In the special case with no magnetostatic field and consequently an isotropic, scalar dielectric constant $\breve{\kappa}$, (4.4.6) becomes

$$\nabla^2\mathbf{E} + \frac{\omega^2}{c^2}\breve{\kappa}\mathbf{E} + \nabla\left[\frac{(\nabla\breve{\kappa})\cdot\mathbf{E}}{\breve{\kappa}}\right] = 0. \tag{4.4.8}$$

If, furthermore, we assume that the wave is initially plane and transverse and $\breve{\kappa}$ changes only in the direction of propagation, then $(\nabla\breve{\kappa})\cdot\mathbf{E} = 0$ and the wave equation reduces to

$$\frac{d^2\mathbf{E}}{dx^2} + \frac{\omega^2}{c^2}\breve{\kappa}(x)\,\mathbf{E} = 0. \tag{4.4.9}$$

Indeed, the adiabatic approximation of Section 4.2 is simply a first-order solution of (4.4.9). For the same special case, (4.4.7) reduces to

$$\frac{d^2\mathbf{H}}{dx^2} + \frac{\omega^2}{c^2}\breve{\kappa}(x)\,\mathbf{H} = \frac{1}{\breve{\kappa}(x)}\frac{d\breve{\kappa}}{dx}\frac{d\mathbf{H}}{dx}, \tag{4.4.10}$$

the magnitudes of **E** and **H** being related by (4.4.1) as

$$H = \frac{j}{\omega\mu_0}\frac{dE}{dx}. \tag{4.4.11}$$

If an *effective* propagation constant $\breve{\gamma}(x)$ is defined such that (Osterberg, 1958)

$$\breve{\gamma}(x) = -\frac{1}{E}\frac{dE}{dx}, \tag{4.4.12}$$

then (4.4.9) requires that $\breve{\gamma}$ satisfy the Riccati differential equation[5]

$$-\frac{d\breve{\gamma}}{dx}+\breve{\gamma}^2+\frac{\omega^2}{c^2}\,\breve{\kappa}(x)=0. \tag{4.4.13}$$

[5] In a homogeneous medium (4.4.13) gives the familiar result $\gamma=\pm j\kappa^{1/2}\omega/c$. The condition for the validity of the adiabatic approximation is then seen to be

$$\left|\frac{d\gamma}{dx}\right|\approx\frac{\omega}{2c}\frac{1}{\kappa^{1/2}}\frac{d\kappa}{dx}\ll\frac{\omega^2}{c^2}\,\kappa,$$

or

$$\frac{1}{\kappa}\frac{d\kappa}{dx}\ll\frac{2\omega}{c}\,\kappa^{1/2}\approx\frac{4\pi}{\lambda}$$

where λ is the local wavelength in the medium. That is, the relative change in κ over a wavelength must be small compared to 4π. The same condition is obtained from (4.4.17).

TABLE 4.1 EFFECT OF INHOMOGENEITY AND ANISOTROPY ON PROPAGATION OF PLANE ELECTROMAGNETIC WAVES (Bachynski, 1960)

Type of medium	Direction of inhomogeneity	Wave type* O	X	L, R
Uniform isotropic $\boldsymbol{\kappa}^{-1}=e$	None	TEM	TEM	TEM
Uniform anisotropic $\boldsymbol{\kappa}^{-1}=\begin{pmatrix} e_\perp & e_\times & 0 \\ -e_\times & e_\perp & 0 \\ 0 & 0 & e_\parallel \end{pmatrix}$	None	TEM	TM	TEM
Inhomogeneous isotropic $\boldsymbol{\kappa}^{-1}=e(\mathbf{r})$	Along initial $\boldsymbol{\gamma}$	TEM	TEM	TEM
	Along initial **E**	TM	TM	TM
	Along initial **H**	TE	TE	TE
Inhomogeneous anisotropic $\boldsymbol{\kappa}^{-1}=\begin{pmatrix} e_\perp(\mathbf{r}) & e_\times(\mathbf{r}) & 0 \\ -e_\times(\mathbf{r}) & e_\perp(\mathbf{r}) & 0 \\ 0 & 0 & e_\parallel(\mathbf{r}) \end{pmatrix}$	Along initial $\boldsymbol{\gamma}$	TEM	TM	TEM
	Along initial **E**	NT	TM	NT
	Along initial **H**	TE	NT	NT

* O=ordinary, X=extraordinary (propagation across field); L, R=left/right-hand (propagation along field); TEM=transverse electromagnetic; TE=transverse electric; TM=transverse magnetic; NT=nontransverse; the propagation coefficient $\boldsymbol{\gamma}$ is in direction of wave normal.

If (4.4.13) can be solved for $\breve{\gamma}(x)$, the wave propagation is given by

$$E(x)=E(0)\exp\left[-\int_0^x \breve{\gamma}(x)\,dx\right]. \tag{4.4.14}$$

In general, (4.4.13) yields two solutions for $\breve{\gamma}$, corresponding physically to waves traveling in both directions. In fact, where $\breve{\kappa}$ is pure real, one solution is the complex conjugate of the other. Reflection and transmission coefficients are obtained by matching boundary conditions in a manner analogous to the uniform slab problem of Section 4.3. For the simple model of a linear variation in electron density, for instance, (4.4.9)

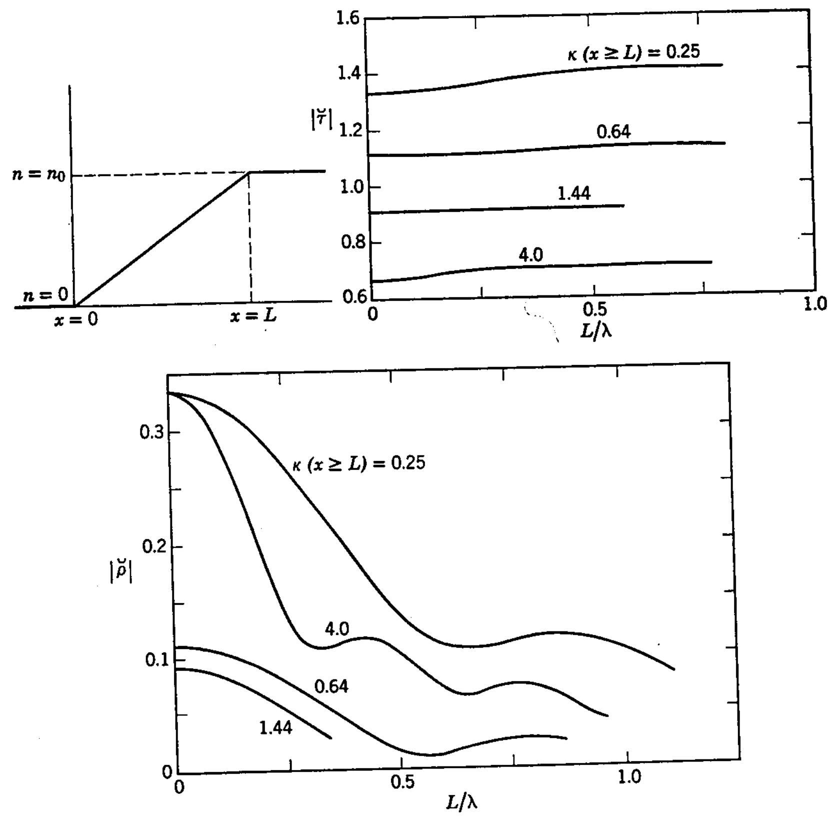

FIG. 4.7 Amplitude reflection and transmission coefficients for a linear-ramp variation of electron density n, as a function of ramp length L for real dielectric constants of the form $\kappa=1-n/n_c$; λ is free-space wavelength. (Reproduced from Albini and Jahn, 1961, by courtesy of the *Journal of Applied Physics*.)

may be solved directly in terms of Airy functions and computations made for linear ramp or trapesoidal profiles (Albini and Jahn, 1961; Wort, 1962). Figure 4.7 illustrates the dependence of reflection coefficient on ramp length and dielectric constant. Numerical calculations for other simple profiles have been made by Taylor (1961), Klein et al. (1961), and Hain and Tutter (1962). Interference effects, arising between reflections from the two sides of an inhomogeneous slab appear to be much more pronounced in the amplitude and phase of the reflected wave than for the transmitted wave. A somewhat similar problem has been considered in connection with tapered waveguides (Johnson, 1959).

4.4.2 ***Anisotropic inhomogeneous plasmas.*** In more general cases it is usually easier to deal with the magnetic vector, since it is always solenoidal. Once **H** is found from (4.4.7), **E** may be obtained from (4.4.2). Consider as a somewhat more general special case an inverse dielectric tensor in the form

$$\breve{\boldsymbol{\kappa}}^{-1} = \begin{bmatrix} \kappa_\perp^{-1} & \kappa_\times^{-1} & 0 \\ -\kappa_\times^{-1} & \kappa_\perp^{-1} & 0 \\ 0 & 0 & \kappa_\parallel^{-1} \end{bmatrix}, \tag{4.4.15}$$

which is appropriate to a cold plasma in a magnetic field directed in the z direction. Further assume that the elements of $\breve{\boldsymbol{\kappa}}^{-1}$ are functions of x only and that propagation is in the x direction with **H**-polarization alternatively in the y or z direction (ordinary or extraordinary waves, respectively). Expansion of (4.4.7) indicates that the magnetic field remains transverse for both cases, whereas (4.4.6) indicates that the electric field is transverse only for the ordinary wave. Assumption of a space-dependent, effective propagation constant analogous to (4.4.12)

$$\breve{\gamma}(x) = -\frac{1}{H}\frac{dH}{dx}, \tag{4.4.16}$$

leads to the differential equation for $\breve{\gamma}(x)$ analogous to (4.4.13)

$$-\frac{d}{dx}(\breve{\kappa}^{-1}\breve{\gamma}) + \breve{\kappa}^{-1}\breve{\gamma}^2 + \frac{\omega^2}{c^2} = 0, \tag{4.4.17}$$

where $\breve{\kappa}^{-1} = \kappa_\parallel^{-1}(x)$ or $\kappa_\perp^{-1}(x)$ for the ordinary and extraordinary wave, respectively. Numerical calculations for this anisotropic case have been made by Hain and Tutter (1962).

The problem of an inhomogeneous cylindrical plasma is again more complex, since the wave equation must be dealt with in cylindrical coordinates. With a plane wave incident upon a cylindrical plasma, it is possible in principle to calculate the phase and amplitude of the scattered wave as a function of scattering angle (King and Wu, 1959). Since these quantities are readily measurable as a function of angle, the inverse problem of deducing the profile from scattering data provides an interesting technique for measuring plasma profiles (Shmoys, 1961; Kerker and Matijević, 1961).

4.5 The geometrical optics of a uniform cylindrical plasma column

A very approximate but useful model of common laboratory plasmas assumes a homogeneous cylindrical plasma several free-space wavelengths (of the probing microwave) in diameter, and yet neglects reflections at the boundary—the geometrical optics limit. The basic parameters of this geometry are defined in Fig. 4.8. The problem is assumed two-dimensional, the elements being of infinite extent normal to the paper. If the plasma is distant by at least a wavelength from the antenna, induction effects can be neglected and the situation treated as a radiation problem. If

$$A/\lambda \gg 1$$
$$D/\lambda \gg 1,$$

geometrical optics is a valid approximation, and we can talk in terms of rays which, except for refraction, travel in straight lines.

4.5.1 ***Transmission loss by refraction.*** We now consider the effect of refraction (Heald, 1959a; Wort, 1963). Since the index of refraction of the plasma (no magnetic field, or parallel polarization) is

$$\mu = (1 - n/n_c)^{1/2} < 1$$

the plasma column constitutes a divergent cylindrical lens. With the help of Fig. 4.9 we compute the refraction of rays in the geometrical-optics limit for a homogeneous plasma with sharp boundaries. The exit

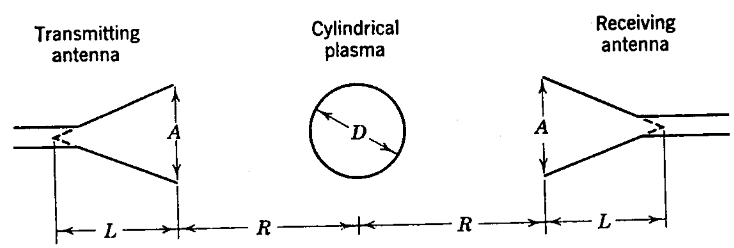

FIG. 4.8 Microwave beam geometry for a cylindrical plasma.

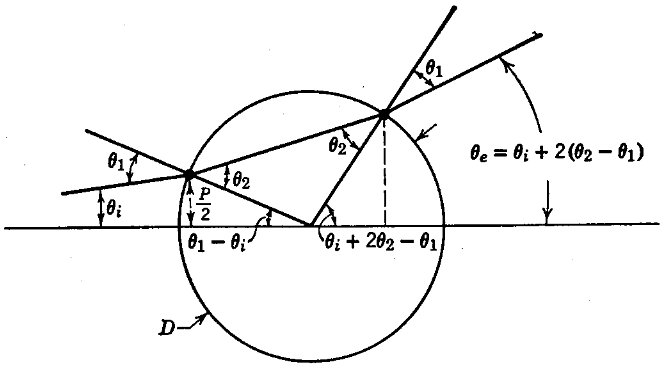

FIG. 4.9 Cylindrical refraction.

angle θ_e is given in terms of the incident angle θ_i and the entrance ordinate $P/2$ by the following simultaneous equations:

$$\theta_e=\theta_i+2(\theta_2-\theta_1)$$

$$\sin(\theta_1-\theta_i)=\frac{P}{D}$$

$$\sin\theta_1=\mu\sin\theta_2 \tag{4.5.1}$$

If now the exit ray is to strike the edge of the receiving aperture, at cartesian coordinates $(R, A/2)$ with respect to the center of the cylinder cross section, we have the following condition on θ_i and $P/2$ for the most divergent ray accepted by the receiving aperture,

$$\tan\theta_e=\frac{A-D\sin(\theta_i+2\theta_2-\theta_1)}{2R-D\cos(\theta_i+2\theta_2-\theta_1)}. \tag{4.5.2}$$

In many cases of practical interest it is reasonable to make small angle approximations. We obtain from (4.5.1)

$$\theta_1-\theta_i=\frac{P}{D}$$

$$\theta_1=\mu\theta_2,$$

and thus

$$\theta_e=2\left(\frac{1}{\mu}-1\right)\frac{P}{D}+\left[2\left(\frac{1}{\mu}-1\right)+1\right]\theta_i. \tag{4.5.3}$$

Setting $m=(1/\mu)-1$, from (4.5.2)

$$(2R-D)\left[2m\frac{P}{D}+(2m+1)\theta_i\right]=A-D\left[(2m+1)\frac{P}{D}+2(m+1)\theta_i\right]. \tag{4.5.4}$$

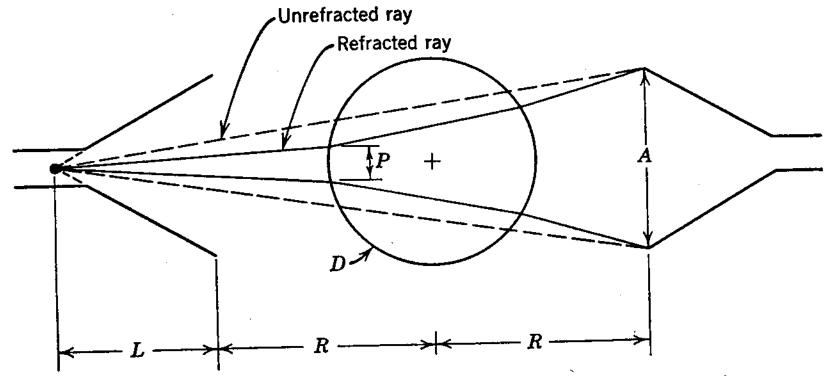

FIG. 4.10 Effect of refraction in geometrical optics approximation.

Solving for P/D, we have

$$\frac{P}{D}=\frac{A-[2(2m+1)R+D]\theta_i}{4mR+D}. \tag{4.5.5}$$

For $\mu<1$ the largest angle involved is $(\theta_i+2\theta_2-\theta_1)$, and the small angle approximation is self-consistent for

$$(2m+1)\frac{P}{D}+2(m+1)\theta_i\ll 1$$

or

$$\frac{P}{D}\ll\frac{1-2(m+1)\theta_i}{2m+1}. \tag{4.5.6}$$

In the geometrical optics limit, with a point source at $-(L+R)$, we have from Fig. 4.10

$$\sin\theta_i=\frac{P}{2(L+R)-D\cos(\theta_1-\theta_i)} \tag{4.5.7}$$

or for small angles

$$\theta_i=\frac{P}{2(L+R)-D}. \tag{4.5.8}$$

Eliminating θ_i in (4.5.5) and rearranging, we have finally

$$\frac{P}{D}=\frac{A[(L+R)-D/2]}{4mR(L+R)+D(L+2R)}. \tag{4.5.9}$$

We recall that $P/2$ is the largest entrance ordinate of rays that pass into the receiving aperture. Therefore, when $P/D\ll 1$ the cylinder is equivalent to a slab of thickness D. With the above evaluation of θ_i the small angle approximations will be self-consistent if from (4.5.6)

$$\frac{P}{D} \ll \frac{2(L+R)-D}{2(2m+1)(L+R)+D} \qquad (4.5.10)$$

or using (4.5.9)

$$A \ll \frac{4mR(L+R)+D(L+2R)}{(2m+1)(L+R)+D/2}. \qquad (4.5.11)$$

Neglecting dissipation in the plasma, we obtain a reduction in amplitude at the receiving aperture because of the loss of highly refracted rays. This (power) transmission ratio is

$$T = \frac{P}{P(\mu=1)} = \frac{D(L+2R)}{4mR(L+R)+D(L+2R)} \qquad (4.5.12)$$

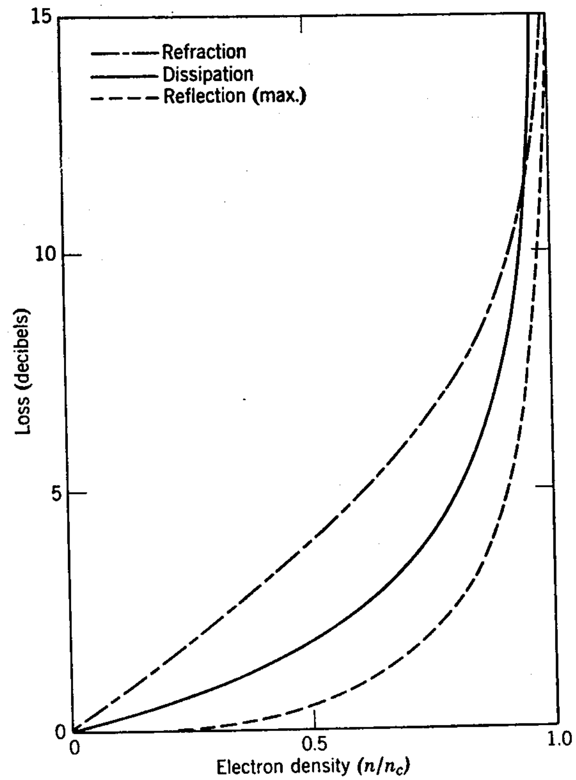

FIG. 4.11 Loss of transmitted amplitude from refraction $4R(L+R)/D(L+2R)=3.6$, dissipation $\nu D/\omega\lambda=0.1$, and reflection.

where we recall that

$$m = \frac{1}{\mu} - 1 = \frac{1}{(1-n/n_c)^{1/2}} - 1 \approx \frac{1}{2}\frac{n}{n_c} + \dots$$

Figure 4.11 shows this transmission loss as a function of electron density for the particular case of

$$\frac{4R(L+R)}{D(L+2R)} = 3.6.$$

4.5.2 ***Other sources of loss.*** For comparison, we compute the dissipative loss in the plasma due to collisions. From (1.3.30), for $n<n_c$ and low dissipation (that is, $\nu^2 \ll \omega_p{}^2 < \omega^2$), this transmission loss is given in decibels by

$$T[\text{dB}] = -8.686\,\alpha D = -\pi(8.686)\frac{n/n_c}{(1-n/n_c)^{1/2}}\frac{\nu D}{2\pi c}, \qquad (4.5.13)$$

for rays passing near the center of the plasma. Figure 4.11 shows this relation for the numerical case

$$\frac{\nu D}{2\pi c} = \frac{\nu}{\omega}\frac{D}{\lambda} = 0.1.$$

For the numerical cases chosen, the refraction loss dominates except very close to the critical density.

Finally, we consider the question of interference effects due to reflections at the sharp plasma–vacuum interfaces. In the usual case of $P/D \ll 1$ the only rays received are those which pass near the center of the plasma, and we can regard the plasma as a slab of thickness D. For the case of lossless slabs, the transmission ratio (4.3.9) becomes

$$T = \frac{1}{1+\left(\frac{1-\mu^2}{2\mu}\right)^2 \sin^2\left(\frac{2\pi\mu D}{\lambda}\right)} \qquad (4.5.14)$$

which varies between

$$\left(\frac{2\mu}{1+\mu^2}\right)^2 < T < 1$$

as the relative phasing of the reflections changes. This maximum transmission loss is also shown in Fig. 4.11.

4.6 The antenna problem

The observed interaction of an electromagnetic wave with a plasma of finite size necessarily implies a "beamed" wave of finite extent and thus depends upon the antenna system used to radiate and receive the wave (Beard et al., 1962). The plane-wave model, which has been tacitly

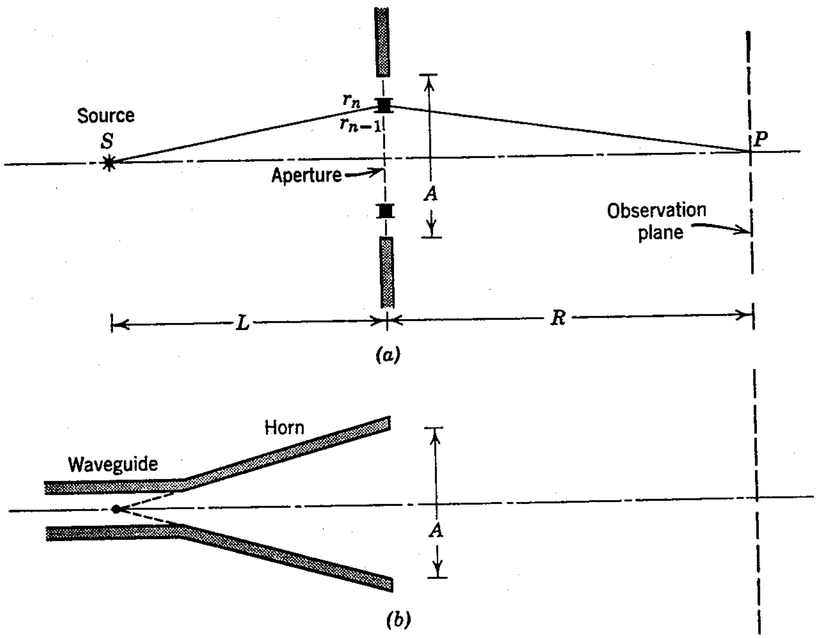

FIG. 4.12 Geometry of the physical optics of (*a*) an aperture, and (*b*) a microwave horn antenna.

assumed in the preceding discussion, is a mathematical idealization which oversimplifies the practical situation, especially when the wavelength is not much smaller than the plasma sample. Therefore, it is useful to review some of the basic principles of diffraction.

4.6.1 ***Fresnel zones.*** Consider a circular aperture, of diameter A, in an opaque screen illuminated with waves from a point S at a distance L to the left, as in Fig. 4.12*a*. We wish to investigate the nature of the radiation field in the vicinity of an observation point P on the axis a distance R to the right. In accordance with elementary Huygens-Kirchhoff-Fresnel diffraction theory, we may divide up the wave front in the aperture into *Fresnel half-period zones*, such that the radiation passing from S to P travels an additional half wavelength for each zone (Andrews, 1960). Specifically, the nth zone is a circular strip, the radius r_n of the outer edge of which is defined such that

$$(L^2+r_n^2)^{1/2}+(R^2+r_n^2)^{1/2}=L+R+n\frac{\lambda}{2}. \qquad (4.6.1)$$

Setting $r_n=A/2$ and assuming $A \ll L$ and R, (4.6.1) may be expanded binomially to obtain

$$n=\frac{A^2}{4\lambda}\left(\frac{1}{L}+\frac{1}{R}\right). \qquad (4.6.2)$$

If the aperture is uniformly illuminated, the contributions of adjacent zones are out of phase and of approximately equal amplitude and, thus, tend to cancel. Insight into the intensity distribution at various observation points (not necessarily on the axis) may be obtained by investigating the number of zones and the fractional area of each zone exposed by the aperture. For instance (Fig. 4.13), the intensity at P on the axis is a maximum for an aperture exposing 1, 3, 5, . . . zones, and a minimum for 2, 4, 6, . . . zones. The intensity at a point off the axis is small if roughly equal areas of odd and even numbered zones are exposed.

To a first approximation the radiation pattern of a horn antenna, of diameter A as in Fig. 4.12*b*, may be described by this analysis (Silver, 1949). We are here interested in only a qualitative description and, therefore, will not be concerned with the modifications required by a rectangular rather than circular aperture, by the polarization of an electromagnetic (transverse) wave, and by nonuniformity of illumination of the horn aperture. However, in passing, it may be noted that for the rectangular aperture with waveguide feed the diffraction field depends upon two factors each of which depends, in turn, on only one of the aperture dimensions—that is, the two dimensions are uncoupled (Schelkunoff and Friis, 1952, Chapter 16). We take A to represent the dimension controlling the radiation pattern of interest (for example, in the plane perpendicular to the axis of a cylindrical plasma as in Fig. 4.10), and

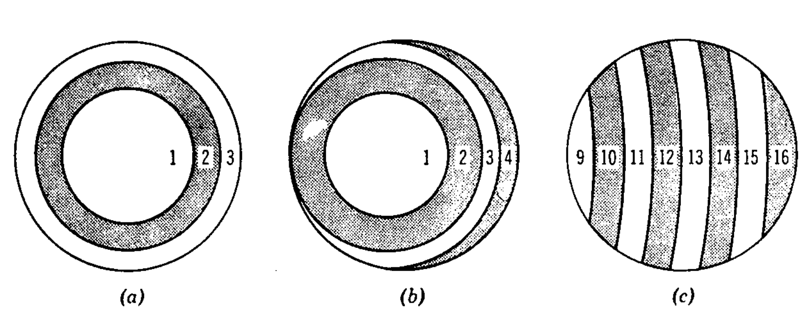

FIG. 4.13 Fresnel zones in a circular aperture; (*a*) on axis, (*b*) slightly off axis, and (*c*) far off axis (enlarged scale). (See also Fig. 9.26.)

ignore the other dimension. Furthermore, we shall assume $L \gg R$ so that L drops out of the analysis and (4.6.2) becomes[6]

$$n = A^2/4\lambda R. \tag{4.6.3}$$

Types of antennas other than horns may also be described in similar terms by suitably choosing an effective aperture dimension A.

If A, R, and λ are such that the number n of exposed Fresnel zones is in the range of one to ten, then strong interference fluctuations are to be

[6] Conversely, it may be noted that the criterion for "optimum" horn design—that is, the choice of A to maximize the gain for a fixed length L—is effectively $n \approx 1$ for $R \gg L$ (Schelkunoff and Friis, 1952).

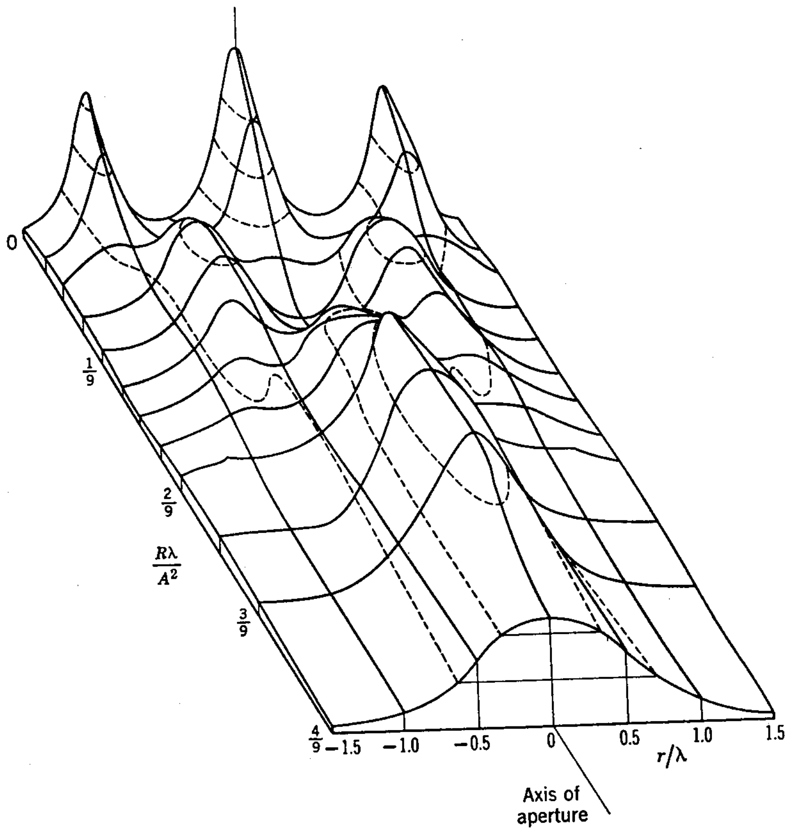

FIG. 4.14 H-plane intensity pattern in the field of a circular aperture, three wavelengths in diameter. (Reproduced from Andrews, 1947, by courtesy of *The Physical Review*.)

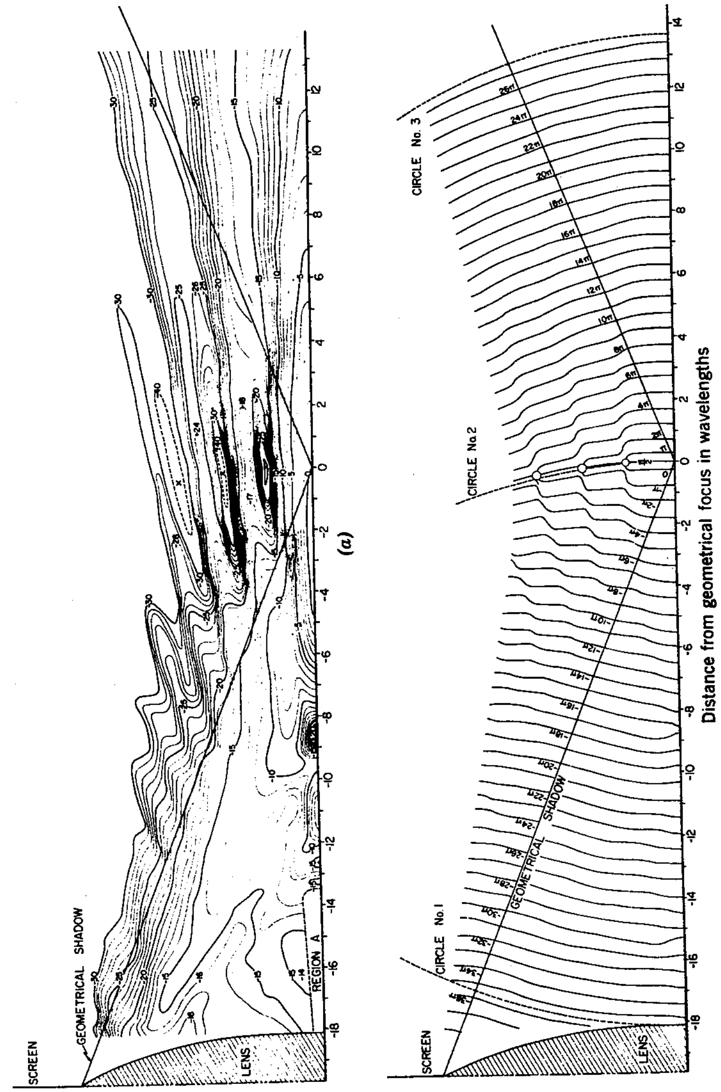

FIG. 4.15 Contours of (*a*) constant intensity, and (*b*) constant phase, in field of a lens 15.5 wavelengths in diameter. (Reproduced from Farnell, 1958, by courtesy of the *Canadian Journal of Physics.*)

expected in the spatial vicinity of the point P. For low-order Fresnel interference, amplitude variations are very large, the field pattern is "choppy" as indicated in Fig. 4.14, and phase anomalies occur (Andrews, 1947, 1950; Linfoot and Wolf, 1956). A further example is shown in Fig. 4.15 (Farnell, 1958).

If n is very large, exclusion of induction fields requires $R \gtrsim \lambda$ and therefore $A \gtrsim 2n^{1/2}\lambda \gg \lambda$, and the intensity distribution near P is essentially that of geometrical optics; that is, uniform intensity falling sharply to zero in the geometrical shadow of the aperture. If a lens of focal length R is inserted at the aperture, a Fraunhofer diffraction pattern is obtained in the plane containing P, as in the familiar problem of the astronomical telescope.

If, on the other hand, n is much less than unity, a Fraunhofer diffraction pattern is obtained at P even without a lens. This is the familiar far-field case of conventional microwave antenna theory. To the extent that

$$n \approx A^2/4\lambda R \ll 1,$$

we have

$$R \gg A^2/4\lambda.$$

This is equivalent to the well-known rule for the far (Fraunhofer) field of an antenna, which is usually written[7]

$$R \gtrsim A^2/\lambda \tag{4.6.4}$$

and signifies that the maximum phase differential between "rays" is less than $\lambda/8$, or that the aperture is less than one-fourth of the first Fresnel half-period zone (Montgomery, 1947). The total angular width of the central maximum of the Fraunhofer diffraction pattern is $2\lambda/A$. Therefore, the spatial width of the central maximum falling on a plane in the far field is

$$(2\lambda/A)R \gtrsim 2A.$$

Thus, if $A \gg \lambda$ the intensity distribution in the vicinity of P is quite smooth over distances of the order of a wavelength, as in the high n case but in contrast to the $1 \lesssim n \lesssim 10$ case. The behavior of the field can be expected to be qualitatively like the far field, up to a range corresponding to the first Fresnel half-period zone $R = A^2/4\lambda$ (Hu, 1961).

4.6.2 ***Collimation.*** It is an interesting property of microwave optics that one can satisfy the Fraunhofer diffraction criterion $R \gtrsim A^2/\lambda$ without the use of collimating lenses as normally required in the optical region. That is, the "far field" of a radiation aperture, or an obstacle, is a much closer distance, in wavelengths, than for similar apertures in the optical case. Therefore, in many situations, far-field theory can be used to describe the microwave field. Meanwhile, the use of lenses becomes less powerful since the focal length F of the lens must be

$$F \lesssim A^2/\lambda \tag{4.6.5}$$

[7] Some antenna engineers use the criterion $R \gtrsim 2A^2/\lambda$, corresponding to $\lambda/16$ or one-eighth zone. Amplitude errors due to interference are then about 2% as opposed to 5% for the criterion given above.

if the focusing effect of the lens is to influence the diffraction pattern appreciably. The so-called f number of the lens is then

$$f = F/A \lesssim A/\lambda. \tag{4.6.6}$$

When the geometrical optics condition $A/\lambda \gg 1$ no longer holds, lens designs of small f number are called for; these show strong aberration and are otherwise impractical. Stated differently, the width of the (Fraunhofer) diffraction pattern at the focus of a lens is

$$(2\lambda/A)F = 2f\lambda \tag{4.6.7}$$

with $f \gtrsim 1$ for practical lenses.

The far-field region can be effectively extended somewhat closer to the antenna aperture by using a lens to partially overcome the diffraction spreading (Sherman, 1962). The angular half-width of the central maximum of the Fraunhofer diffraction pattern is λ/A. In geometrical optics a ray leaving the edge of an aperture of width A at this angle appears to originate at a point located a distance $A^2/2\lambda$ on the source side of the aperture, and therefore the insertion of a lens of focal length $F = A^2/2\lambda$ will render this extreme ray parallel to the axis. The f number of such a lens is

$$f = A/2\lambda, \tag{4.6.8}$$

agreeing closely with the upper limit of (4.6.6).

Table 4.2 summarizes the characteristics of the radiation field for various regimes of the parameters. The best collimation ($\sim\lambda$) is obtained

TABLE 4.2 FIELD PATTERNS AND COLLIMATION OF ANTENNAS

Number of zones in aperture	Small aperture $A/\lambda \sim 1$	Large aperture $A/\lambda \gg 1$
$n \gg 10$	Induction field region	Normal geometrical ray optics (collimation $\sim A$ without lens; $\sim\lambda$ with lens)
$1 < n \lesssim 10$	Induction field region	Fresnel interference, "choppy" intensity distribution (collimation $\sim A$)
$n < 1$	Fraunhofer diffraction radiation pattern (collimation $2\lambda R/A \gtrsim A$)	

in the $A/\lambda \sim 1$, $n < 1$ case (antenna far field) and the $A/\lambda \gg 1$, $n \gg 10$ case with lens (geometrical optics). The latter, however, is a strongly converging wave passing through a focus. It appears best to design the experiment so as to avoid the low-order region ($1 \lesssim n \lesssim 10$). If the number of Fresnel zones is either very large or small throughout the space occupied by plasma and receiving antenna, then the illumination will be fairly uniform and the phase fronts well-behaved.

4.6.3 ***Optimization of antennas.*** Let us assume that we are given the diameter D of a cylindrical plasma column and the wavelength λ with which we are to probe it. We further assume that λ, determined by the electron density range to be measured and perhaps the availability of short-wavelength instrumentation, is small compared to D but by no means negligible. Since we wish to obtain a reasonable average of the electron density independent of refraction (and diffraction) by the plasma, we wish to achieve maximum collimation of the microwave beam so that it effectively passes along a diameter. We have seen from a geometrical optics point of view that when $\mu < 1$ the divergent lens action improves the effective collimation by refracting nondiametric rays out of the receiving aperture. However, because of the danger of reflection from such extraneous obstacles as the vacuum system walls, and because of the desire to conserve feeble millimeter-wave power, we wish to maximize the power in received diametric rays and minimize it in nonreceived and/or nondiametric rays. That is, we wish to minimize the insertion loss between antennas while ensuring that most of the radiation passes close to the axis of the plasma (Heald, 1959a).

The most clear-cut situation is when $D \gg A \gg \lambda$, which conforms closely to infinite-slab, geometrical-optics conditions. However, our interest is in the case where perhaps $1 \lesssim D/\lambda \lesssim 10$. If $A > D$, appreciable energy passes around the plasma, reducing sensitivity and severely complicating interpretation. With $D \gtrsim A \gtrsim \lambda$, in order to avoid induction field effects and Fresnel-zone interference effects, we must have the plasma located in the far (Fraunhofer) field of the antennas, $R \gtrsim A^2/\lambda$.

It is a well-known rule of antenna engineering that for a pair of antennas to be located in the far-field region, by the usual A^2/λ criterion, the minimum insertion loss is of the order of 16dB (Montgomery, 1947). Since only about two per cent of the radiated power is received, the probability of interference from spurious reflected signals is high. We are, therefore, interested in pushing as close to the near field (Fresnel zone number $n \sim 1$) as possible without encountering severe amplitude and phase disturbances from interference. This leads to the alternative of small (nondirective) antennas relatively close to the plasma or large (directive) antennas farther back.

The concentration of rf energy produced in the field of a horn antenna depends upon two factors: the width of the wavepacket launched, and the angle of spread of the wave. Empirical plots of intensity contours in the field of millimeter horn antennas indicate that one half of the energy is confined within a beam width

$$W = \left[\left(\frac{aA}{2}\right)^2 + \left(\frac{b\lambda R}{A}\right)^2\right]^{1/2} \tag{4.6.9}$$

where a and b are correction factors depending on geometry and aperture illumination and departing only slightly from unity. For a given λ and R, this is minimized when

$$A = \left(\frac{2b}{a}\lambda R\right)^{1/2} \tag{4.6.10}$$

giving

$$R = \frac{a}{2b}\frac{A^2}{\lambda}$$

$$W_{min} = (ab\lambda R)^{1/2}. \tag{4.6.11}$$

This condition corresponds to an aperture of about one half a Fresnel half-period zone at R. The insertion loss between two such antennas spaced $2R$ apart is about 8dB, depending upon the other dimension of the antenna aperture. Sometimes mechanical constraints of the apparatus will prescribe R, in which case A is determined by (4.6.10). If both A and R are at the experimenter's disposal, it is necessary to consider the role of the diameter D of the plasma column. The relative beam size W/D varies as $R^{1/2}/D$, whereas the relative spreading of the field over the plasma

$$\frac{D}{W}\left(\frac{\partial W}{\partial R}\right)_{W_{min}}$$

varies as D/R. Since we wish $W \ll D \ll R$, we arbitrarily take

$$D = (W_{min}R)^{1/2} = (ab\lambda R^3)^{1/4}. \tag{4.6.12}$$

Recapitulating, given D and λ and assuming $a = b = 1$, we choose

$$R = \left(\frac{D}{\lambda}\right)^{1/3} D$$

$$A = (2\lambda R)^{1/2} = \sqrt{2}\left(\frac{\lambda}{D}\right)^{1/3} D. \tag{4.6.13}$$

This heuristic argument is founded on the vague assumption that there is some virtue in minimizing the beam width at the plasma by choice of A and then compromising in the choice of R such that

$$\frac{D}{W_{min}} = \frac{R}{D}.$$

The effect is to prescribe a situation in which the plasma is located slightly inside the conventional far-field boundary. We have seen, however, that under these conditions diffraction anomalies should not be very severe. Note that when $D/\lambda \gg 1$, $R \ll D^2/\lambda$ and, therefore, the plasma approximates an infinite slab as far as diffraction is concerned. By reciprocity and symmetry arguments, we conclude that transmitting and receiving antennas should be identical.

The preceding discussion has been based on the assumption of simple horn antennas without lenses. It has also assumed a "long" horn ($L \gtrsim A^2/\lambda$) and $L \gtrsim 2R$, which may be impractical. Thus, two uses for lenses emerge: (*1*) to permit a less-than-long horn, in accord with conventional practice; and (*2*) to focus the beam or at least over-collimate to compensate partially for diffraction. If a horn is "long," its far-field ($R > A^2/\lambda$) pattern cannot be appreciably narrowed by addition of a lens. However, in the previous section we have discussed the use of a lens to focus the energy at a distance $R \lesssim A^2/\lambda$. The suggestion has been made to use converging lenses focused at the plasma axis (Boyd, 1959). This is chiefly based upon the geometrical-optics argument that all rays pass diametrically through the plasma, thereby removing the refraction and sampling difficulties of the "plane-wave" approach. If $A/\lambda \gg 1$ so that a good focus can be obtained, and if this focus ($\sim \lambda$) is small relative to the plasma, $D/\lambda \gg 1$—that is, a good geometrical optics situation—this procedure has merits (Papoular and Wegrowe, 1961). However, in this case, the relative rf field strength becomes very high in the vicinity of the focus, so that nonlinearities in the rf properties of the plasma may be troublesome. If, on the other hand, $D/\lambda \sim 1$, the so-called Gouy phase anomalies in the vicinity of the focus (Fig. 4.15) could severely complicate the interpretation (Linfoot and Wolf, 1956; Bekefi, 1957; and Farnell, 1958). In this case, it appears that if lenses are to be used they should be focused at the opposite antenna or beyond (Christian and Goubau, 1961). Further discussion of the practice of using lenses can be found in Sections 6.4 and 9.3.

Because of the perturbation that thick dielectric windows (glass, mica, quartz, etc.) make on the field of a millimeter-wave antenna (Redheffer, 1949), it is often useful to locate the vacuum seal at a convenient point back in the waveguide so that the antennas are wholly within the vacuum system. Such window design follows standard practice as used in microwave tube output windows and waveguide pressurizing windows; examples are given in Section 9.6. Alternatively, care must be taken to provide matching structures at the vacuum walls (Jahn, 1962).

4.6.4 ***Validity of the geometrical-optics, slab model.*** Since the geometrical-optics, plane-slab model is particularly convenient to analyze,

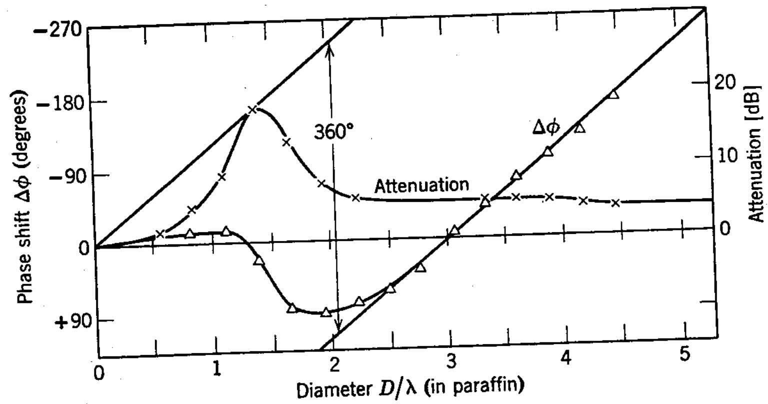

FIG. 4.16 Phase shift and attenuation as a function of cylinder diameter in paraffin analog experiment (Rosen, 1949). Wave **E**-field parallel to cylinder axis. Dimensions normalized to wavelength in the medium of the antennas: **H**-plane aperture of horn 3.1; **E**-plane aperture 2.6; axial length of horn (to apex) 6.8; horn separation 13.4. Measurement frequency 35 Gc.

it is of interest to investigate the validity of this model for the more practical case of a cylindrical plasma. In addition, since the nearness of the antennas, as well as of extraneous objects such as vacuum system walls, severely complicates theoretical analysis, it is often most effective to perform an analog experiment (Warder, Brodwin, and Cambel, 1962; Iams, 1950; and Lashinsky, 1963).

A plasma, with dielectric constant less than unity, can be simulated by cutting holes in a large block of low-loss dielectric, in which a scaled antenna system is imbedded. In one such experiment the phase shift and insertion loss were measured for various size cylindrical holes cut in

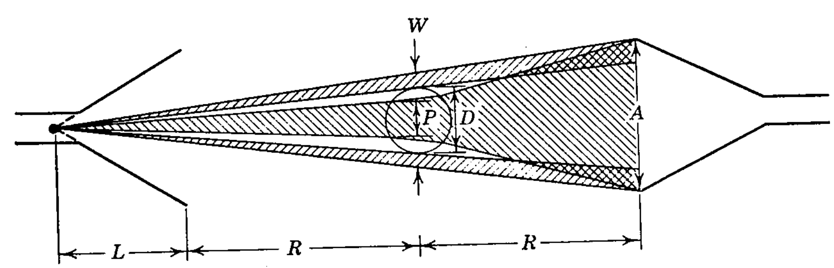

FIG. 4.17 Propagation through a dielectric cylinder, small compared to effective microwave beam.

paraffin ($\kappa = 2.25$) (Rosen, 1959). This dielectric constant ratio corresponds to a plasma of 0.56 critical density. The antenna system was chosen for a plasma diameter of about four wavelengths in accordance with the design criteria of Section 4.6.3, the prototype system having an insertion loss of approximately 8dB in vacuum. Typical results are shown in Fig. 4.16. For cylinder diameters greater than about three wavelengths, the observed phase shift differs negligibly from what would be expected for a plane slab, except for the loss of a full wavelength. This latter effect can be explained as the result of interference between the wave passing through the cylinder and the wave passing around it. Using the notation of Fig. 4.17, we regard the wave entering the receiving aperture as composed of two components: (*a*) the wave passing through the cylinder of

amplitude $(P/W)^{1/2}$
phase $2\pi(\mu-1)D/\lambda$

(neglecting internal interference effects), where $\mu < 1$ is the refractive index of the cylinder (air) relative to the paraffin, and λ is the wavelength in the paraffin; and (*b*) the unperturbed wave passing around the cylinder of

amplitude $(1-D/W)^{1/2}$
phase 0.

W is the effective beam width at the plasma,

$$W = \frac{L+R}{L+2R} A; \tag{4.6.14}$$

and from (4.5.9)

$$\frac{P}{D} \approx \frac{A[(L+R)-D/2]}{4\left(\frac{1}{\mu}-1\right)R(L+R)+D(L+2R)}. \tag{4.6.15}$$

The resultant wave is then

$$\left(\frac{P}{W}\right)^{1/2} \exp[j2\pi(\mu-1)D/\lambda] + \left(1-\frac{D}{W}\right)^{1/2} \exp(j0) \equiv C \exp(j\Delta\phi) \tag{4.6.16}$$

where C and $\Delta\phi$ are the amplitude and phase shift of the resultant wave. We have

$$C = \left\{\frac{P}{W} + \left(1-\frac{D}{W}\right) + 2\left(\frac{P}{W}\right)^{1/2}\left(1-\frac{D}{W}\right)^{1/2} \cos[2\pi(\mu-1)D/\lambda]\right\}^{1/2}, \tag{4.6.17}$$

$$\Delta\phi = \tan^{-1} \frac{\left(\frac{P}{W}\right)^{1/2} \sin[2\pi(\mu-1)D/\lambda]}{\left(\frac{P}{W}\right)^{1/2} \cos[2\pi(\mu-1)D/\lambda] + \left(1-\frac{D}{W}\right)^{1/2}}. \tag{4.6.18}$$

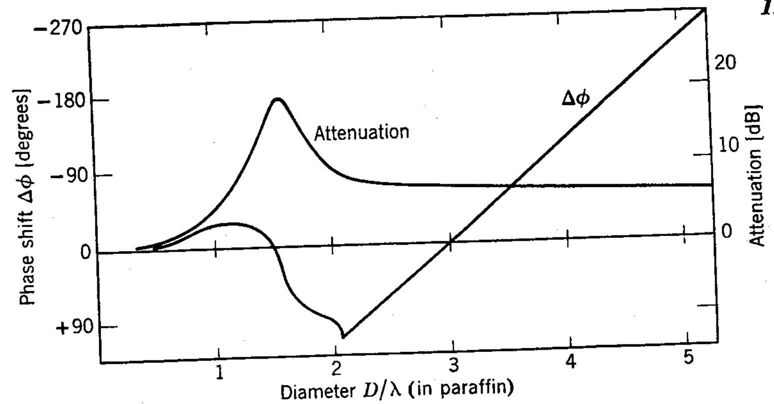

FIG. 4.18 Results of simple geometrical optics theory for the conditions of Fig. 4.16, exhibiting "loss" of 360°.

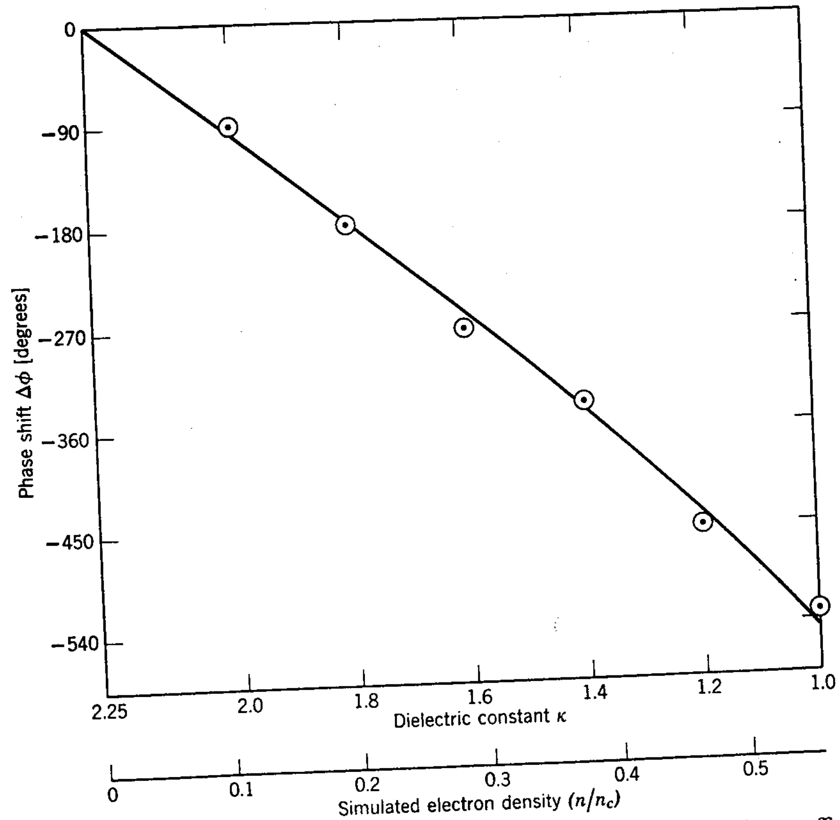

FIG. 4.19 Phase shift as a function of dielectric constant of cylinder in paraffin-analog experiment, simulating plasma of varying density. Cylinder diameter 4.6 wavelengths.

The theoretical C and $\Delta\phi$ are plotted in Fig. 4.18 for parameters corresponding to the experimental conditions of Fig. 4.16. In order to obtain these relations for C and $\Delta\phi$, several small-angle approximations have been made, diffraction was completely neglected, and interference effects inside the cylinder were disregarded. In spite of the crudity of the geometrical optics analysis, the numerical agreement is reasonably good.

This "lost-wavelength" effect could cause misleading results in a plasma experiment in the uncommon situation in which the plasma is created with a small diameter ($<2\lambda$) which subsequently grows larger.[8] More commonly, the plasma is created with a relatively large diameter ($>3\lambda$) and then grows denser (due to increased ionization) or smaller (due to some form of magnetic compression). In these cases, the transition from the vacuum (no plasma) phase-shift condition, as the plasma develops, appears to be unambiguous. By inserting rods of various known dielectric constants in a fixed diameter hole in the paraffin environment, the data of Fig. 4.19 was obtained, simulating varying plasma densities (Rosen, 1959). On the basis of this study, we conclude that the slab analysis is satisfactory for a cylindrical plasma diameter of at least three wavelengths, provided the antenna system is chosen judiciously.

[8] The expanding-diameter situation could occur during a plasma decompression event or an expanding cylindrical shock.

CHAPTER 5

Guided wave propagation

5.0 Introduction

The effects of finite plasma dimensions on wave propagation were discussed in Chapter 4. The boundaries were found to cause reflections and refraction of transmitted waves and, in some cases, to affect the radiation patterns of antennas. In most cases, the boundaries led to problems, rather than being beneficial to the propagation experiments.

In the present chapter, we discuss another class of bounded plasmas; in this case, boundaries are essential to the wave propagation. Resonant cavities and waveguides have metallic walls that carry currents and, thus, set up propagation modes. The electromagnetic fields penetrate the enclosed plasma, whose conductivity, in turn, affects the mode cut-off frequency. Measurements of wave phase shift or resonant frequency and loaded Q then can be related to the plasma properties.

Plasmas having vacuum or dielectric boundaries can support space-charge-wave modes and, thus, can act as waveguides. Certain space-charge-wave modes propagate along the plasma surface (surface waves), while others are carried within the plasma (body waves). When a magnetic field is present, the waves tend to be a combination of both types.

Electromagnetic waves and spacecharge waves may propagate simultaneously along the same bounded plasma. Under certain conditions, the different wave types may couple to one another but, in general, the coupling coefficients are rather small.

5.1 Measurements on plasmas contained in resonant cavities

The resonance properties of a cavity containing a lossy dielectric can be stated in terms of Q